Mechanism for the disassembly of excited ^{16}O projectiles into four alpha particles

R. J. Charity, J. Barreto,* L. G. Sobotka, D. G. Sarantites, D. W. Stracener, A. Chbihi,† and N. G. Nicolis
Department of Chemistry, Washington University, St. Louis, Missouri 63130

R. Auble, C. Baktash, J. R. Beene, F. Bertrand, M. Halbert, D. C. Hensley, D. J. Horen, C. Ludemann, M. Thoennessen,‡ and R. Varner
Oak Ridge National Laboratory, Oak Ridge, Tennessee 37830
(Received 31 July 1991; revised manuscript received 14 July 1992)

The decay of excited ^{16}O projectiles into the four alpha particle exit channel has been investigated. The projectiles, with bombarding energies of $E/A = 25$ MeV, were excited through peripheral interactions with ^{159}Tb target nuclei. A 4π counter was used to detect both the projectile alpha particles and the light charged particles evaporated from the target nucleus. Criteria for selecting true $^{16}O \rightarrow 4\alpha$ events with the minimum contamination from incorrectly identified events were examined. The distribution of relative angles between the four alpha particles in their center of mass frame was compared to simulations of ^{16}O decay by sequential decay mechanisms. The relative angles were shown to be consistent with a sequential evaporation mechanism if a nonzero angular momentum is assumed for the excited projectile. The momentum distribution of the alpha particles in the reaction plane was examined and found to be anisotropic for high projectile excitation energies. This anisotropy was shown to be consistent with Coulomb interactions between the first emitted alpha particle and the target nucleus, which would indicate that the lifetime of the projectile is very short, on the order of 10^{-22} s.

PACS number(s): 25.70.Lm, 25.70.Mn

I. INTRODUCTION

The decay of nuclei into many pieces is a topic of much interest at present. Mechanisms proposed to explain the disintegration process include both prompt breakup scenarios and models where the fragments are emitted sequentially. Also theories based on both statistical and dynamical ideas are available. It is important in studies of many fragment events to find clear signatures for the different modes of disassembly. Such signatures may be obtained from correlations between the fragments. If the fragments produced by the disassembly process are initially in close proximity and their subsequent interaction is dominated by their mutual Coulomb repulsions, then one expects a suppression of events with small relative velocities. On the other hand, for a sequential process, if the time steps between emissions are sufficiently long, then the emitted fragments will not experience any mutual interactions. Small relative velocities will therefore not be suppressed. Trockel *et al.* [1] measured the correlation between intermediate mass fragments produced in violent collisions of ^{18}O ($E/A = 84$ MeV) on ^{nat}Ag and ^{197}Au targets as a function of their relative velocities and deduced a time interval between fragment emissions of $(0.6\text{–}3.0)\times10^{-21}$ s.

The mechanism for the breakup of $E/A = 32.5$ MeV ^{16}O projectiles excited through peripheral interactions with a ^{197}Au target has been studied by Harmon *et al.* [2, 3]. They measured the distributions of relative angles between the pieces produced in the breakup and compared these to predictions from prompt, sequential, and dynamical models.

Also some studies [2, 4] have attempted to use event shape analysis [5] as a signature to distinguish the two classes of decay mechanisms. Such analyses are extremely sensitive to finite particle number effects [6]. Nevertheless, some tentative statements have been made. Harmon *et al.* [2] find that the event shape analysis indicates a sequential decay mechanism in agreement with their conclusion from the analysis of the relative angles mentioned above. Cebra *et al.* [4] conclude that the fragmentation process for central collisions in the $^{40}Ar + {}^{51}V$ reaction is consistent with the sequential mechanism at $E/A = 35$ MeV. For higher bombarding energies, the event shape analysis gives results intermediate between predictions for the prompt and sequential mechanisms.

For projectile disassembly, correlations between the projectile fragments and the target nucleus are of interest. Interactions between the target and projectile fragments can modify the energy and emission pattern of the fragments. Glässel *et al.* [7] have studied sequential fission-like reactions and interpreted deviations of the separation velocity between the fission fragments as due

*On leave from Instituto de Física da UFRJ–21945 RJ, Brazil.
†Present address: Laboratoire Ganil, Caen, France.
‡Present address: National Superconducting Cyclotron Laboratory, Michigan State University, East Lansing, Michigan 48824.

to the proximity of a third fragment during the fission decay. They used the magnitude of this effect to estimate the time scale of the fission-like process.

In this work, we report on a study of the disassembly of ^{16}O projectiles into the four alpha particle exit channel. The projectiles, with bombarding energies of $E/A = 25$ MeV, were excited through peripheral interactions with the ^{159}Tb target nuclei. The present work is more extensive than previous studies [2, 8] of ^{16}O breakup in that the measurements were performed with a nearly 4π detection system allowing the decay of the excited target nucleus to be studied as well. The detection of all light charged particles proved useful in distinguishing events with four alpha particles originating from the projectile from other events with four alpha particles. Correlations between the alpha particles and between the alpha particles and the target nucleus were used to infer the decay mechanism and the time scale for the decay.

This paper is divided into six sections. In Sec. II, Monte Carlo simulations of the disassembly process are presented. Predicted relative angle distributions and the dependence of the target proximity effect on the decay width and angular momentum of the projectile are discussed. Section III describes the experiment, while the selection of ^{16}O$\rightarrow 4\alpha$ events and their possible contamination by other 4α events are discussed in Sec. IV. The experimental relative angle distributions and the observation of a target proximity effect are discussed in Sec. V and compared to predictions obtained from the simulations. Finally, the conclusions of this work are summarized in Sec. VI.

II. SIMULATIONS

A. Relative angle distributions

To study the disassembly of excited ^{16}O projectiles and to learn the signatures of the various types of decay modes, Monte Carlo simulations were performed. The sequential decay of an ^{16}O projectile into four alpha particles can proceed by two possible routes. Either the alpha particles can be sequentially evaporated, forming in turn a ^{12}C and then a ^{8}Be intermediate, or the decay sequence can be initiated by the fission of the projectile into two ^{8}Be fragments. Rather than allowing both of these possibilities to be included in a single sequential simulation as in Ref. [2], two separate simulations were performed. The former of these routes will be called sequential evaporation and the latter sequential fission.

For the sequential evaporation simulation, alpha particle emissions from the ^{16}O projectile and the ^{12}C intermediate were described by the statistical model. The Hauser-Feshbach formalism was used to choose the emitted alpha particle's kinetic energy and orbital angular momentum and also the excitation energy and angular momentum of the daughter. If the level densities of the daughters (i.e., ^{12}C and ^{8}Be) for the two evaporation steps are taken from the Fermi gas model and the emission directions are chosen isotropically, then the predicted relative angle distribution is shown in Fig. 1

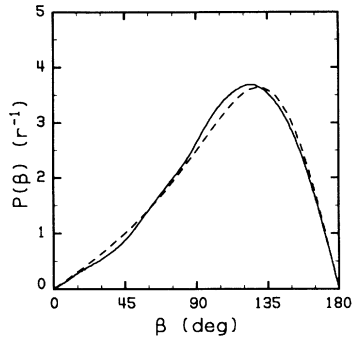

FIG. 1. Simulated probability distributions of the six relative angles between the four alpha particles produced in the disassembly of ^{16}O projectiles with excitation energy of 40 MeV. The dashed curve was obtained with the sequential evaporation simulation using Fermi gas model level densities for both the ^{12}C and ^{8}Be intermediates and an initial excitation energy of 40 MeV. The solid curve was obtained with the random simulation.

(dashed curve). This particular simulation is for a projectile with 40 MeV of excitation energy and zero angular momentum. The predicted distribution was found to be relatively insensitive to the initial excitation energy and angular momentum. This distribution is very similar in form to that obtained by the sequential simulation in Ref. [2] where the transition-state formalism was used instead of the Hauser-Feshbach formalism and the level density of the transition states were taken from the Fermi gas model. Thus, the choice as to which statistical model formalism to use in the simulations is not important.

The relative angle distribution generated with this sequential evaporation simulation is almost identical to a random distribution of relative angles with the constraint of momentum conservation. To illustrate this, relative angles were obtained by first choosing four points randomly in a spherical volume. The relative angles were constructed from the center of mass of these four points and the resulting distribution (solid curve) is compared to the above described sequential simulation in Fig. 1. The two distributions are very similar, indicating that momentum conservation is determining the shape of this sequential distribution.

The use of Fermi gas model level densities for such light nuclei as ^{12}C and ^{8}Be is questionable and therefore must be investigated. For a ^{16}O excitation energy of 40 MeV, which is typical of that found in this work (see Sec. V) and in Ref. [2], the ^{12}C daughter will be formed with an average excitation energy of 22 MeV. The density of known levels for ^{12}C [9] peaks around 19 MeV indicating the presence of many undiscovered levels with energy above 19 MeV. Therefore, the use of a continuous level density seems appropriate at 20 MeV of excitation energy and above. When Fermi gas model level densities are assumed, the average excitation energy of the ^{8}Be daughter after the evaporation of another alpha particle is ≈ 5 MeV. As the first (2_1^+) and second (4^+) excited states of ^{8}Be occur at $E^*= 3.04$ and 11.4 MeV [10], respectively, the use of a Fermi gas model level density

for this daughter nucleus is inappropriate. These considerations suggest that a reasonable approach for the sequential evaporation simulation is to employ Fermi gas model level densities for the ^{12}C daughter, but only the known levels should be considered for the ^{8}Be daughter. Furthermore, as only the four alpha exit channel is of interest, only the known alpha-unstable levels of ^{8}Be were included in the simulation.

In what has been described above, the emission direction at each step of the decay was assumed random as in Ref. [2]. However, with a proper treatment of angular momentum, the emission directions will be correlated. As an example, consider the decay of a ^{12}C daughter of zero angular momentum into an alpha particle and a ^{8}Be fragment in its first excited state. The angular momentum of this excited state is $2\hbar$ which ultimately becomes the orbital angular momentum of the two alpha particles when the ^{8}Be decays. However, as the original ^{12}C had zero angular momentum, the orbital angular momentum of the alpha particle evaporated from it must be equal in magnitude but opposite in direction to the ^{8}Be angular momentum vector. Thus, the orbital angular momentum vectors of the three alpha particles must be either parallel or antiparallel with respect to each other. Therefore classically, these alpha particles must all be emitted in the same plane perpendicular to these angular momentum vectors. Hence, the distribution of relative angles will be more concentrated near 0° and 180° as compared to when the two emission directions were chosen randomly. In the sequential evaporation simulation there are three emission directions, so the triple correlation function is needed. The quantum mechanical treatment of the triple correlations between emission directions from Refs. [11, 12] was used in the simulations.

The relative angle distributions predicted from the sequential evaporation simulation, which included ^{8}Be structure and a quantum treatment of correlations, are shown in Fig. 2 for E^{*}=40 MeV and two initial ^{16}O angular momenta, $I = 0\hbar$ (dashed curve) and $5\hbar$ (solid curve).

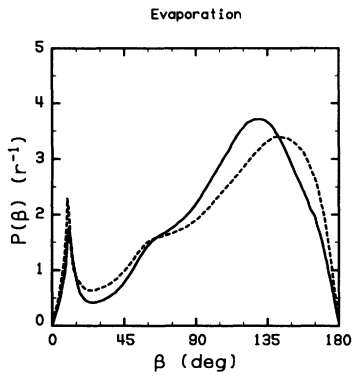

FIG. 2. Predicted probability distributions of relative angles obtained with the sequential evaporation simulation, including a quantum mechanical treatment of correlations between emission directions. Predictions are shown for initial angular momenta of $I = 0\hbar$ (dashed curve) and $I = 5\hbar$ (solid curve) with an initial excitation energy of 40 MeV.

Unlike the distributions obtained without the ^{8}Be structure and correlations (see above), there is a strong dependence on angular momentum. Also, a sharp peak is very prominent at small relative angles ($\beta \approx 10°$). This peak is associated with pairs of alpha particles produced from the decay of ^{8}Be fragments in their ground states. A small shoulder at $\beta \approx 60°$ is associated with the decay of the first excited state of ^{8}Be. Increasing the initial ^{16}O angular momentum from $I = 0\hbar$ to $5\hbar$ has two effects. Firstly, the intensity in the peak corresponding to ^{8}Be ground state decay was reduced. Decay into the first two excited states of ^{8}Be is favored as I increases because these states have angular momenta of $2\hbar$ and $4\hbar$, respectively. Secondly, the correlations are reduced at $I = 5\hbar$. This is somewhat surprising as one generally expects correlations to increase with angular momentum and to be minimal at zero angular momentum. However, the correlations are stronger for $I = 0\hbar$ as the decay was more likely to proceed through a path containing a ^{12}C intermediate of zero angular momentum which decays into the first or second excited state of ^{8}Be as described in the example above. The relative angle distribution for $I = 0\hbar$ is subsequently enhanced at $\beta \approx 0°$ and 180°. For the $I = 5\hbar$ simulation, the effect of the correlation is much smaller and the distribution is more similar to that obtained with random emission directions.

The quantum treatment of these correlations was very time consuming in terms of computer usage. However, the correlations can be more rapidly treated by using a semiclassical approximation. At each decay step, classical angular momentum vectors were obtained from the angular momentum quantum numbers chosen from the Hauser-Feshbach formalism. A triangle of vectors, corresponding to the angular momentum of the decaying system and the daughter nucleus and the orbital angular momentum of the evaporated alpha particles, was constructed assuming the magnitudes of the vectors were given by the corresponding quantum numbers. The emission direction of the alpha particle was then chosen randomly in the plane perpendicular to its orbital angular momentum vector. Figure 3 shows a comparison of the relative angle distributions derived with the quantum (solid curve) and semiclassical (short-dashed curve) treatments and for isotropic emission (long-dashed curve) for $I = 0\hbar$ and E^{*}=40 MeV. The semiclassical approximation predicts slightly more correlations between emission directions than the quantum treatment. However, the semiclassical approximation is quite good except for values of β close to 0° and 180°.

For the sequential fission simulation, the projectile fissions into two ^{8}Be fragments each of which later decay into two alpha particles. The excited states of the ^{8}Be fragments, and their separation velocity, were again chosen using the Hauser-Feshbach formalism and a quantum mechanical treatment of correlations between the fission axis and the two ^{8}Be decay axes was used. The predicted relative angle distributions are shown in Fig. 4 for $I = 0\hbar$ (dashed curve) and $5\hbar$ (solid curve). These predicted distributions contain many peaks corresponding to different combinations of the excited states of the two ^{8}Be fragments. The most prominent of these peaks are labeled in

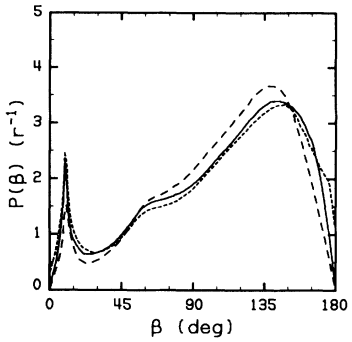

FIG. 3. Comparison of relative angle distributions obtained with the sequential evaporation simulation for an initial angular momentum of $I = 0\hbar$ and an initial excitation energy of 40 MeV. The solid curve was obtained with a quantum mechanical treatment of correlations between emission directions, the short-dashed curve using the semiclassical approximation, and the long-dashed curve was obtained assuming uncorrelated emission directions.

Fig. 4. For example, the first peak in the predicted distributions at β=8° labeled as g.s.-(g.s.,2_1^+) is associated with the alpha particles produced by the decay of the ground state of a ^{8}Be when the other ^{8}Be fragment was formed in its ground state or in its first 2^+ state. The levels listed inside the parentheses refer to the other ^{8}Be fragment, the one not producing the two alpha particles which give the correlation. Prominent peaks are also obtained from the decay of the first, second, and third 2^+ states (2_1^+, 2_2^+, 2_3^+). The first 4^+ state is very broad and does not produce a prominent peak. The peak labeled g.s.-g.s. is also associated with events where two ^{8}Be fragments are formed in their ground states, but the relative angle here is between alpha particles originating from different ^{8}Be fragments. The position of these peaks will move as the excitation energy changes because the separation velocity between the ^{8}Be fragments will change. The relative distributions predicted with the evaporation and fission simulations are quite distinctive and should be easily distinguished if the resolution for measuring relative angles is sufficient.

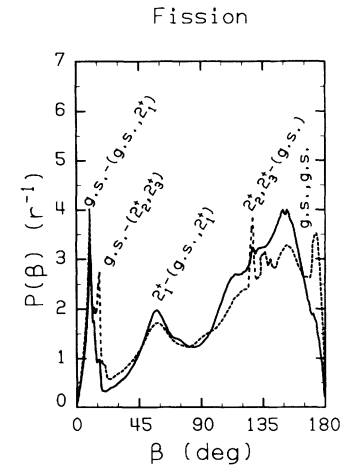

FIG. 4. Predicted probability distributions of relative angles between alpha particles obtained with the sequential fission simulation. Predictions are shown for initial angular momenta of $I = 0\hbar$ (dashed curve) and $I = 5\hbar$ (solid curve) with an initial excitation energy of 40 MeV. The prominent peaks in these distributions are labeled to indicate the levels of ^{8}Be from which the alpha particles were produced. The levels of the other ^{8}Be fragment are indicated in the parentheses.

In simulating the prompt decay of the projectile, Harmon *et al.* [2] have followed the prompt decay recipe of López and Randrup [5]. In this recipe, initial positions of four alpha particles are chosen randomly inside a source volume. The initial velocity vectors of the alpha particles are then chosen from a microcanonical distribution. The classical trajectories of the alpha particles under their mutual Coulomb interactions are then followed until the velocity vectors approach their asymptotic values. The initial relative angle distribution obtained from the microcanonical distribution is similar to the random distribution discussed previously. The repulsive Coulomb interactions between the alpha particles modify this relative angle distribution tending to suppress small relative angles and enhance intermediate values producing a subsequent narrowing of the relative angle distribution [2].

However, the above recipe ignores nuclear final state effects and the symmetrization of the outgoing wave functions for identical particles. For alpha particles, both the nuclear and symmetrization final state effects work in the opposite direction to that from the Coulomb interaction. To determine the magnitude of these effects, the two-body momentum correlation function

$$1 + R = \frac{\sigma(p_1, p_2)}{\sigma(p_1)\,\sigma(p_2)} \tag{1}$$

was investigated, where $\sigma(p_1, p_2)$ and $\sigma(p_i)$ are the two-body and single particle emission probabilities. For two fragments emitted initially uncorrelated from a source, the correlation function arising from two-body final state interactions between these fragments can be calculated from the Koonin-Pratt formula [13–15]:

$$1 + R = \int d^3r_1\, d^3r_2\, g(r_1)\, g(r_2)\, |\Phi_{p_1 p_2}(r_1, r_2)|^2 \tag{2}$$

where $g(r)$ is the initial space distribution of an emitted particle and Φ is the relative wave function between the fragments. The formula given above [Eq. (2)] assumes the fragments are emitted promptly, i.e., there was no time delay between the two emissions.

The functions $g(r)$ were taken the same as for the López-Randrup prompt recipe, i.e., the initial positions were randomly selected within a spherical volume. The radius of this volume was taken as 3.8 fm, 40% larger than the radius of a cold ^{16}O. This source radius is needed to reproduce the prompt simulation of Ref. [2]. Calculated two-body correlation functions are plotted in Fig. 5 as functions of the final relative momentum between the fragments Δp. The short-dashed curve indicates the distribution obtained when only a Coulomb potential between the fragments was considered when calculating Φ. The Coulomb interaction suppresses events

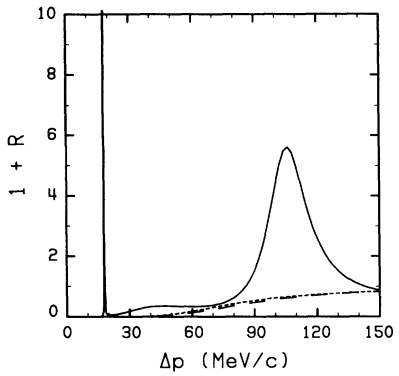

FIG. 5. Two-body correlation functions calculated for alpha particles emitted promptly from a source of radius 3.8 fm. The long-dashed curve gives the results obtained when only the Coulomb interaction between the fragments is considered. The short-dashed curve indicates the prediction when the Coulomb interaction and the symmetrization of the outgoing wave function are included. The solid curve also includes the effect of a realistic nuclear potential between the fragments.

with small relative momenta, consistent with the suppression of small relative angles in the previously mentioned prompt simulation. The long-dashed curve indicates the effect of symmetrizing the wave function. The symmetrization reduces the suppression a little, but this is not a large effect. The solid curve shows the effect of including a more realistic α-α potential. The potentials of Refs. [16] and [17], both of which reproduce elastic scattering phase shift data, were investigated. The solid curve in Fig. 5 was obtained with the potential from Ref. [17], but the result obtained with the other potential was similar.

The two-body correlation function indicates that the most important interaction between promptly emitted alpha particles is resonance scattering. The large peaks at Δp=20 and 100 MeV/c correspond to scattering through the ground and the first excited state (2_1^+) of ^{8}Be. If the potential of Ref. [16] is used, then a broader peak at higher Δp is also obtained corresponding to the 4^+ state. The correlation function not only shows the expected peaks in the regions of the strong resonances, but substantial differences between calculations with and without a nuclear potential also exist in regions where there are no resonances. For example, in the region $30<\Delta p<60$ MeV/c, where there are no resonances, the suppression of correlations is greatly reduced relative to that predicted with only a Coulomb interaction. This illustrates that the use of the López-Randrup prompt simulation is inadequate for exit channels containing more than one alpha particle.

A proper treatment of prompt four alpha particle emission requires higher order correlations. However, one might suspect that at high excitation energies, where the probability of finding a pair of alpha particles with small relative velocities in the region of these resonance scattering peaks is small, two-body correlations would be adequate. To estimate the probability that a pair of alpha particles generated from a thermal source is involved in resonance scattering, one can multiply the Δp spectrum predicted by a microcanonical distribution by the two-body correlation function in Fig. 5. The area associated with the resonance scattering peaks relative to the total area of the new spectrum gives an estimate of this probability. For an excitation energy of 40 MeV, one obtains that, on average, three pairs of alpha particles are involved in resonance scattering interactions per event. Considering that there are only six permutations of alpha particle pairs, if taken seriously, two alpha particles must each be involved in two separate resonance scattering interactions per event. This clearly indicates the need to consider higher order correlations at this excitation energy.

B. Target proximity

Information on the time scale of the decay process or its "promptness" can be extracted from studying the effect of the target proximity on the decay. Prompt decays might be expected to occur in the immediate vicinity of the target and thus the emission angles of the alpha particles will be affected by the Coulomb field of the target. The presence of the field has two effects. This can be illustrated by performing a first order Taylor expansion of the target's electric field around the projectile at position $\mathbf{r}_0$:

$$\mathbf{E}(\mathbf{r}) = E_0\frac{\mathbf{r}_0}{|r_0|} - E_0\frac{\delta\mathbf{r}_\parallel}{|r_0|} + E_0\frac{\delta\mathbf{r}_\perp}{|r_0|}, \tag{3}$$

where

$$E_0 = \frac{Z_t e}{|r_0|^2}, \tag{4}$$

$$\mathbf{r} = \mathbf{r}_0 + \delta\mathbf{r}_\parallel + \delta\mathbf{r}_\perp, \tag{5}$$

$\delta\mathbf{r}_\parallel$ and $\delta\mathbf{r}_\perp$ are displacement vectors parallel and perpendicular to $\mathbf{r}_0$ and $Z_t e$ is the charge on the target nucleus. The first term is a uniform field which accelerates all Z/A =1/2 fragments equally. The other terms give rise to a force similar to the tidal force in gravity only now, as the total force is repulsive, they produce a compressional force in the direction parallel to $\mathbf{r}_0$ (second term) and try to pull apart the projectile in the direction perpendicular to this (third term). The result of these two terms is to make the momentum distribution of alpha particles anisotropic. Those particles emitted perpendicular to $\mathbf{r}_0$ will, on the average, have an increased momentum, while the momentum of those emitted parallel to $\mathbf{r}_0$ will be decreased on average. For particles emitted at intermediate angles, the net effect of the two terms will also be a focusing of the momentum vectors towards perpendicular directions.

One must also appreciate that $\mathbf{r}_0$ rotates (in the laboratory or center of mass frame) as the projectile, and later the projectile fragments, deflect in the Coulomb field of the target. The direction of the momentum anisotropy should reflect the orientation of the projectile-target axis

when the projectile decays rather than the asymptotic direction to the projectile fragment center of mass. For a sequential decay, the decay process is extended in time so the subsequent anisotropy of the momentum distribution will be the combined effect of all the steps. However, the magnitude of the first order terms in Eq. (3) decreases rapidly, as $|r_0|^{-3}$, and hence the anisotropy will be dominated by the anisotropy of the first emitted particle. To look for this anisotropy, the following momentum tensor was considered:

$$T_{ij} = \frac{1}{4N} \sum_{l=1}^{N} \sum_{k=1}^{4} \frac{3 p_i^{lk} p_j^{lk}}{\langle |p|^2 \rangle^l}. \quad (6)$$

The index l is over all events where N is the total number of events in the analysis. The index k is over the alpha particles in an event and p_i^{lk} is the ith component of the kth fragment's momentum vector in the center of mass frame of the projectile fragment in the lth event. The quantity $\langle |p|^2 \rangle^l$ is the average squared magnitude of the four alpha particles' momentum vectors in the lth event. The z axis is defined as the asymptotic axis between the target and the center of mass of the alpha particles and the x axis is defined to lie in the reaction plane such that the orbital angular momentum vector of the target and projectile lies along the y axis. With this definition of the momentum tensor, an isotropic distribution will be associated with the identity matrix. For an anisotropic momentum distribution, the magnitude and direction of the momentum anisotropy can be obtained by diagonalizing the tensor.

Even if there is no target proximity effect, some anisotropy in the momentum distribution may be expected if the projectiles have, on average, an aligned angular momentum. The anisotropy generated by an aligned angular momentum favors in-plane emission relative to emission out of the reaction plane. The proximity effect can be isolated from this effect by looking only at the anisotropy of the in-plane components of the tensor. Simulations were performed to study the target proximity effect assuming sequential evaporation decay with the semiclassical treatment of angular correlations. The trajectories of the target, projectile, and later the projectile fragments were followed after the separation of the target and projectiles using classical mechanics and assuming only Coulomb interactions between these particles. The time interval after this separation up until the emission of the first alpha particle was taken from the exponential distribution:

$$P(t) \propto \exp\left(\frac{-\Gamma t}{\hbar}\right), \quad (7)$$

where Γ is the decay width of the ^{16}O projectile. The time intervals between the emissions of the first and second alpha particles and between the second emission and the breakup of the ^{8}Be were correspondingly taken from exponential distributions determined by the decay widths for the ^{12}C and ^{8}Be intermediates. For the ^{8}Be levels, the measured decay widths listed in Ref. [10] were used. For the ^{12}C intermediate, the same decay width as for the ^{16}O system was assumed for simplicity, although if the ^{12}C decay width is smaller than this value, as might be expected, the predicted anisotropy will also be smaller. However, the above assumption is useful as the two decay widths may not be that dissimilar and also that the largest contribution to the anisotropy comes from the first emitted alpha particle and thus the sensitivity to decay width of the ^{12}C intermediate is not as large.

The anisotropy was calculated as a function of Γ for an initial projectile excitation energy of 40 MeV and where the total kinetic energy plus Coulomb potential of the projectile and target in the reaction center of mass is 263 MeV. The results are presented as the ratio of the two in-plane eigenvalues of the momentum tensor $R_{\rm in}$=T_{33}/T_{11}, where the eigenvalue T_{33} was taken to correspond to the eigenvector which is located in the quadrant between the z axis and the x axis. The direction of the anisotropy is given by the angle θ_z between the eigenvector corresponding to T_{33} and the z axis. These are plotted in Fig. 6 as a function of Γ. Predictions are shown for two initial angular momenta of the ^{16}O fragment, $0\hbar$ (circles) and $5\hbar$. For the latter case, the direction of the angular momentum vector was assumed either aligned perpendicular to the reaction plane (squares) or isotropic (triangles). The predictions for $R_{\rm in}$ show little dependence on the magnitude and alignment of the angular momentum. However, the eigenvalue for the out-of-plane eigenvector is dependent on these quantities. The ratio $R_{\rm out}$=T_{22}/T_{33} ranged from unity for $I = 0\hbar$ or no alignment to 0.35 for $5\hbar$ of aligned angular momentum,

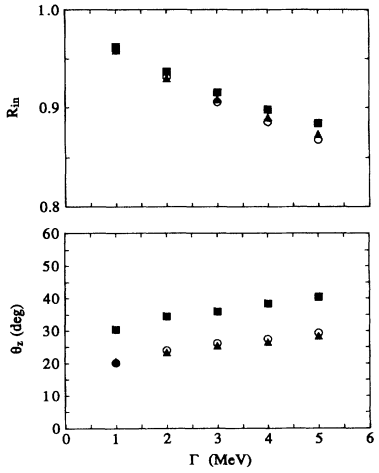

FIG. 6. The predicted dependence of the momentum tensor characteristics on the decay width of the projectile for a projectile excitation energy of 40 MeV and a total kinetic energy of 263 MeV. The quantity $R_{\rm in}$ is the ratio of the two in-plane eigenvalues and the angle θ_z gives the orientation of in-plane eigenvectors relative to the z axis, the asymptotic axis between the center of mass of the projectile fragments and the target. The open circles indicate predictions obtained with zero projectile angular momentum ($I = 0\hbar$) while the solid squares and triangles represent predictions for $I = 5\hbar$ with the alignment of the angular momentum vector being out-of-plane and isotropic, respectively.

with no observed dependence on Γ. Thus, the quantities $R_{\rm in}$ and $R_{\rm out}$ give independent information on the values of Γ and the aligned angular momentum.

For $I = 0\hbar$, the angle θ_z reflects the orientation of the target-projectile axis at the time the first alpha particle is emitted. It increases with increasing Γ (see Fig. 6) approaching, for very large values of Γ, the orientation of the target-projectile axis as they start to separate. Whenever an alpha particle is emitted with nonzero orbital angular momentum, its emission direction will undergo a rotation as it approaches its asymptotic direction. This extra rotation must be considered when discussing θ_z. The value of θ_z for $I \neq 0$ now reflects the orientation of the projectile-target axis when the projectile decays plus an average effect of the extra rotations. If the projectile's angular momentum is not aligned (triangles), then the extra rotations, on average, cancel and the value of θ_z obtained is similar to that obtained for $I = 0\hbar$ (circles). However, if the projectile angular momentum is aligned (squares), the extra rotations are, on average, nonzero and add to the value of θ_z. This explains the larger values of θ_z obtained in Fig. 6 for the simulation with aligned angular momentum.

III. EXPERIMENTAL METHOD

The experiment was performed at the Holifield Heavy-Ion Research Facility of the Oak Ridge National Laboratory. Beams of ^{16}O projectiles with energy E/A = 25 MeV impinged on a ^{159}Tb target of thickness 632 μg/cm^2. Projectile fragments and other light charged particles emitted in the reactions were detected and identified with the Dwarf Wall/Ball Plastic-CsI scintillator array. A detailed description of this array is contained in Ref. [18]. Briefly, the array consists of 104 counters arranged to cover ≈85% of the laboratory solid angle. Scattering angles from approximately 4° to 32° were covered by the more finely grained Dwarf Wall detector array, while the Dwarf Ball detectors subtended the more backward angles. Each scintillator detector could identify protons, deuterons, tritons, alpha particles, ^{3}He and heavier ions. Energy calibrations for protons were performed using elastic and inelastic scattering from a ^{12}C target. The energy calibration for alpha particles was obtained from these proton calibrations using the empirical relationship given in Ref. [18]. In front of the most forward ring of Dwarf Wall counters ($4° \lesssim \theta_{\rm lab} \lesssim 12°$), metal foils (≈450 mg/cm^2 Pb plus ≈10 mg/cm^2 Ta) were placed to stop elastically scattered projectiles. This resulted in a threshold of ≈44 MeV for alpha particles in these counters. All other counters had thresholds of 4 MeV or less for alpha particles. All events triggering a Dwarf Wall counter were recorded on magnetic tape and analyzed off-line.

IV. EVENT SELECTION

The recorded events were examined off-line to select those which were compatible with the oxygen projectile disassembling into four alpha particles. Care must be taken to avoid contamination by incorrectly identified events, e.g., the detection of three alpha particles originating from the projectile and one evaporated from the target nucleus. As a first step, candidate ^{16}O→4α events were selected by requiring that four, and only four, alpha particles were detected in the Wall array ($4° \lesssim \theta_{\rm lab} \lesssim 32°$). For each detected alpha particle, a laboratory angle corresponding to the central angle of the detector was assigned [19] and the velocity vector of the center of mass of the four alpha particles was then obtained. This velocity, in correctly identified events, is the velocity of the excited projectile after its interaction with the target nucleus. Values ranging from the beam velocity to half this value were observed.

A. Angular distributions of Ball particles

If the primary reaction channel for correctly identified candidate events contains just two bodies, then all the particles detected in the Ball array must originate from the decay of the excited target nuclei. Only ≈20% of the candidate 4α projectile fragments are in coincidence with charged particles detected in the Ball counters. This is not surprising since the dominant decay mode of the target nuclei is expected to be neutron evaporation. For the range of reconstructed projectile velocities, the target nuclei should be moving very slowly with laboratory velocities of less than 0.35 cm/ns. The angular emission of these particles should thus be approximately isotropic in the laboratory frame assuming very little spin is transferred to the target nucleus. The experimental angular distributions for these charged particles are displayed in Fig. 7. Rather than the expected nearly flat behavior, these angular distributions are all strongly forward peaked and are not consistent with evaporation from the target nucleus. However for angles greater than 90°, the distributions are significantly flatter.

The angular distributions indicate that either some of the candidate events are incorrectly identified or that the interaction between the target and projectile nuclei is more complex than assumed. In either case, it is useful

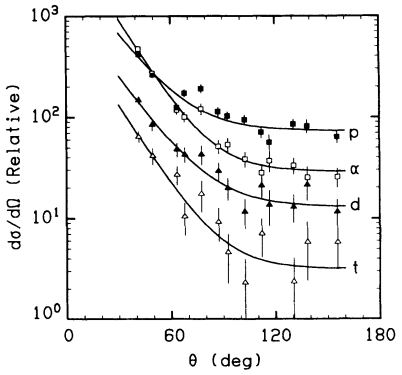

FIG. 7. Relative laboratory angular distributions of protons, deuterons, tritons and alpha particles detected in the Ball counters for events where four, and only four, alpha particles were detected by the Wall counters. The curves guide the eye.

to try to reject such events. Events in which a charged particle is detected in one of the forward Ball counters ($\theta_{lab}<90°$) are more likely to be of this nature; consequently, all such events were removed from the sample of candidate events. Note that this condition does not greatly reduce the number of candidate events as most candidate events were not in coincidence with any charged particle detected in the Ball counters.

The above discussion indicates the advantage of 4π detector systems for studies of this type. Knowledge of the full event characteristics allow cleaner samples of projectile breakup events to be obtained. The above rejection criterion of course not only rejects "bad events" but also some valid events. Our sample is thus biased against events with large target excitation energies as these are more likely to emit charged particles.

Finally, the nature of the rejected "bad events" is not clear. It is possible that they are associated with projectile breakup events in which the primary reaction mechanism is not two body. For example, some of the forward emitted charged particles may correspond to preequilibrium emission from the target nucleus. In such a case, the rejection of these events further biases the selected event sample. However, if these rejected "bad events" are not associated with projectile disassembly, but are from another class of reaction, then their rejection does not contribute a bias. It is important to understand the influence of such biases in order to extract the partition of excitation energy between the target and projectile as attempted in Ref. [8].

B. Multiplicities of Ball particles

As a further check as to the fraction of incorrectly identified candidate events, the magnitude of the particle multiplicities detected in the Ball counters was compared to the expectation for target evaporation. Note that as events in which a charged particle was detected in the forward half of Ball are rejected, the comparison will be for the back half of the Ball where the angular distributions in Fig. 7 are almost flat and are consistent with target evaporation. The spectrum of reconstructed target excitation energy is indicated by the thick-lined histogram in Fig. 8. Target excitation energies of up to ≈200 MeV were observed. Due to the resolution of the detecting apparatus, a few events were encountered where the reconstructed target excitation energy was negative. Any comparison of the predicted multiplicities must consider the effect of this resolution.

Figure 9 shows the detected mean multiplicities of protons, alpha particles, deuterons, and tritons as a function of the reconstructed target excitation energy for various gates on the reconstructed projectile velocity. These multiplicities show a rapid increase with increasing target excitation energy as expected for evaporation. The multiplicities for different projectile velocity gates at the same reconstructed target excitation energy are equal within the statistical error and thus consistent with decay from a fully equilibrated system whose decay is independent of its mode of formation.

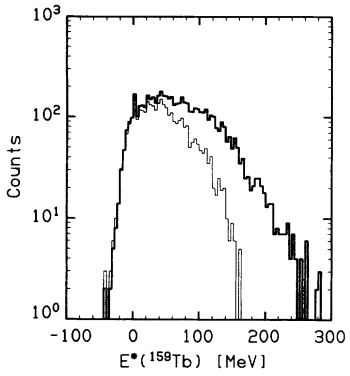

FIG. 8. Reconstructed target excitation energy distributions. The thick-lined histogram was obtained from all selected $^{16}O \rightarrow 4\alpha$ events while the thin-lined histogram corresponds to events where all the alpha particles have laboratory velocities greater than 4.5 cm/ns.

The measured multiplicities are compared to statistical model predictions. The decay widths for particle emission were calculated from the Weisskopf formalism. Inverse cross sections were obtained from the incoming wave boundary condition model [20] using the real part of

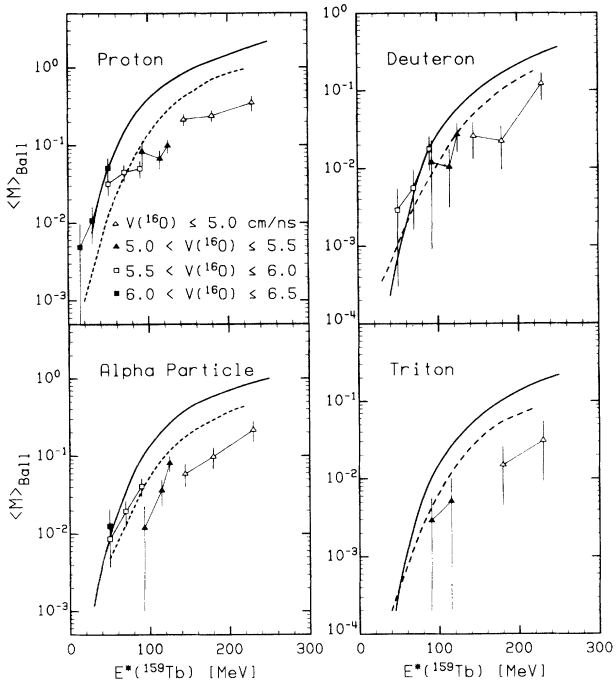

FIG. 9. Multiplicities as a function of the reconstructed target excitation energy of protons, alpha particles, deuterons, and tritons detected in the backward hemisphere of the Ball for events where four, and only four, alpha particles were detected by the Wall counters and no other particles were detected in the forward hemisphere of the Ball. The solid curves indicate statistical model predictions of the particle multiplicities evaporated from the target nucleus. The dashed curves indicate the predicted multiplicities once the effect of the incomplete detector angular coverage and the selection criteria are considered.

global optical model potentials for neutrons [21], protons [22], alpha particles [23], deuterons [24], and tritons [25]. Evaporation from the target nucleus was followed until its excitation energy was depleted. The predicted mean multiplicities are indicated by the solid curve in Fig. 9. However, these values should not be compared to the experimental results since the criteria for selecting the candidate events imposed large corrections to the predicted multiplicities. These corrections were extensively studied using Monte Carlo simulations which will be discussed in Sec. V A. The predicted mean multiplicities of detected fragments for events which pass the identical selection criteria as the candidate events are indicated by the dashed curves in Fig. 9. These multiplicities are also plotted against the target excitation energies reconstructed in the simulations and thus contain the effects of the detector's energy and angular resolutions. The predicted multiplicities show the same rapid increase with target excitation as the experimental results. The agreement between these multiplicities is quite good for low target excitation energies, but at the higher excitation energies, the predicted multiplicities are larger than the values for the candidate events. This may indicate a problem with event selection or with the statistical model predictions at the higher excitation energies. However, the region of disagreement occurs only for the tail of the reconstructed target excitation energy distribution in Fig. 8. For the bulk of the data [$E^*(^{159}Tb)<150$ MeV], the predicted and measured multiplicities are in agreement.

Events where alpha particles evaporated from the target nucleus or from some intermediate source are incorrectly identified as one of the four alpha particles originating from the projectile should lead to low values of the reconstructed projectile velocity as such alpha particles have velocities much less than the beam velocity. Incorrect identification should therefore be a greater problem at the larger kinetic energy dissipations and thus larger reconstructed target excitation energies. This may explain the deviation of the measured and predicted multiplicities at large excitation energies in Fig. 9. As an extra criterion for removing such events, one can insist that the four alpha particles detected by the Wall counters have velocities above a typical value associated with target evaporation. This extra criterion was considered when constructing the relative angle distributions.

The average laboratory velocity of alpha particles emitted forward from a compound nucleus formed in a fusion reaction is estimated to be 4.0 cm/ns. The velocity for alpha particles emitted forward from excited target nuclei formed in more peripheral reactions will be less than this. Thus, the removal of events with alpha particles of velocity 4.5 cm/ns or less should eliminate most of the incorrectly identified events which may still be in the sample. The effect of insisting that all the candidate alpha particles have laboratory velocities greater than 4.5 cm/ns (65% of the beam velocity) is illustrated in Fig. 8. The new reconstructed target excitation energy distribution is indicated by the thin-lined histogram in the figure. The extra condition has completely removed the tail of the distribution above 150 MeV for which the predicted and measured multiplicities were in disagreement. Of course this extra criterion will also reject some real $^{16}O \rightarrow 4\alpha$ events and further biases the event sample against those with large target excitation energies.

V. DISCUSSION

A. Monte Carlo simulations

In order to compare the experimental relative angle distributions of the alpha particles to those of the simulations, the distortions due to the detector limitations must be included. To this end, extensive Monte Carlo simulations were performed taking into account the decay of both the projectile and the target nuclei. The projectile fragment was allowed to decay into four alpha particles following one of the recipes described in Sec. II. The recoiled target nucleus was also allowed to decay by an evaporative cascade of light particles as discussed in Sec. IV B. All emitted light charged particles were then passed through the detector filter. Only those particles whose paths intersected a counter and whose energy was above the appropriate detection threshold were kept. The remaining particles in a simulated event were then checked to see if they satisfied the same criteria used for selecting $^{16}O \rightarrow 4\alpha$ events experimentally: four, and only four, alpha particles detected, each in a separate Wall counter, and no other particles detected in the forward Ball counters. Events with more than one fragment in the same Wall counter were rejected as they were in the analysis of the experimental events.

For simulated events which satisfy the selection criteria, the angles corresponding to the center of the detecting counter were assigned to the detected alpha particle as was done for the experimental events. Also a 5% uncertainty was introduced in the energy of these fragments to take into account the energy resolution of the counters [18]. The velocity, angle, and excitation energy of the projectile and target were then reconstructed. The simulated multiplicities of charged particles detected in the Ball as a function of the reconstructed target excitation energy for the selected events are plotted in Fig. 9 and discussed in Sec. IV B. These predictions were not sensitive to the mode of the projectile disassembly.

In order to perform reliable simulations, reasonable estimates of the distributions of the excited projectile and target nuclei after their primary interaction must be assumed. The scattering angle and excitation energy distributions of the projectile were estimated as a function of the total kinetic energy loss (TKEL) in the primary reaction. The corresponding quantities for the target nucleus were then calculated from conservation laws. These distributions and the TKEL distribution were initially taken as those of the experimentally reconstructed quantities. After running the simulations, the efficiency of the detecting apparatus was estimated and then used to correct the distributions of the experimental reconstructed quantities. For example, the efficiency as a function of the reaction TKEL was calculated by dividing the distribution of the reconstructed TKEL for the "detected" events in the simulation by the primary distribution as-

sumed in the simulation. This efficiency was then used to correct the experimentally obtained spectrum and the resultant spectrum was used as the primary distribution in the simulation to obtain an improved estimate of the efficiency. This procedure was performed simultaneously for the other distributions and after a couple of iterations, the simulated "detected" and the experimentally measured spectra were found to be identical within the statistical errors.

The measured and final corrected TKEL distributions are compared in Fig. 10. The efficiency for identifying $^{16}O \rightarrow 4\alpha$ events depends on the angular coverage and the thresholds of the detecting apparatus and on the criteria used to select these events. From Fig. 10, this efficiency is at best 10% for intermediate values of TKEL. For larger values of TKEL, the efficiency drops rapidly as the target nucleus becomes more excited, emitting non-negligible numbers of light particles and which, if detected in the Wall or the forward Ball counters, cause the event to be rejected. The efficiency also drops rapidly for small values of TKEL as a large number of the alpha particles are emitted in the 0° to 4° angular range where there are no counters. This dependence of the efficiency on TKEL causes the corrected and measured distributions to be quite different. The corrected distribution has features which are expected for dissipative collisions, though it should be remembered that this distribution is not representative of all projectile-like fragments but only those which decay via the 4α exit channel. The large peak for small values of TKEL can be attributed to quasielastic scattering. Actually only the tail of the quasielastic peak is observed as the 4α exit channel has a threshold of $\approx$22 MeV. For larger values of TKEL, the corrected distribution increases in value. This may be associated with the deep-inelastic peak.

Examples of the measured and corrected excitation energy and emission angle distributions of the projectile are shown in Fig. 11 for two bins of TKEL. As expected for dissipative collisions, the more strongly damped collisions are less focused around the beam axis. Also note that the measured and corrected excitation energy distributions are very different in shape for the TKEL<50 MeV bin. This emphasizes the fact that to obtain any information about excitation energy sharing between the target and projectile, the efficiency of the detecting apparatus must be well known.

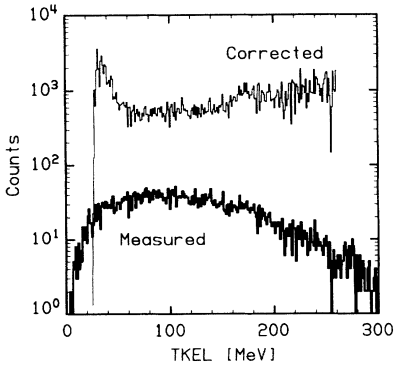

FIG. 10. The measured (thick-lined histogram) and corrected (thin-lined histogram) distributions of reconstructed total kinetic energy loss for the selected $^{16}O \rightarrow 4\alpha$ events.

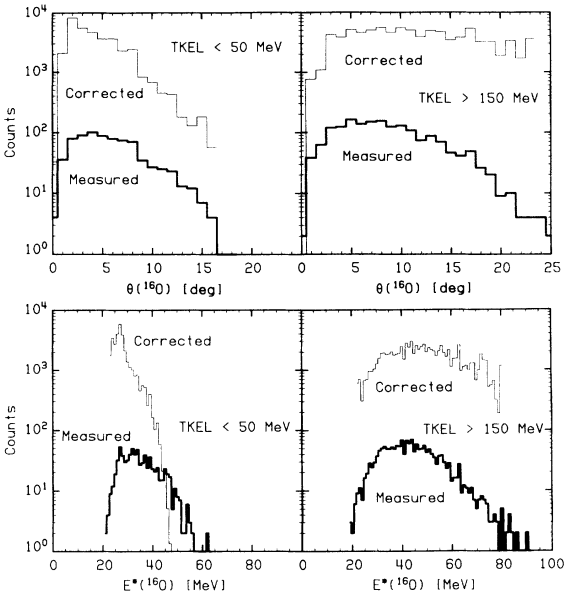

FIG. 11. The measured (thick-lined histograms) and corrected (thin-lined histograms) distributions of reconstructed projectile laboratory angle and excitation energy for two bins of TKEL.

The simulations allow for some incorrect identification of events as no check is made to determine whether all four alpha particles detected in the Wall originated from the projectile. It is possible for one of the projectile alpha particles to miss the Wall counters while an alpha particle evaporated from the target nucleus hits one. However, the level of incorrect identification in the simulations was minimal ($\approx$2%). There may, of course, be other sources of incorrectly identified events which are not included in the simulation.

B. Relative angle distributions

The inclusion of the detecting apparatus has a large effect on the simulated relative angle distributions. There are two effects, firstly, the rejection of events which do not meet the experimental selection criteria and, secondly, the angular and energy resolution associated with reconstructing the relative angles of selected events. The first of these effects has the largest influence on the predicted distributions. To illustrate this, predicted raw (solid) and "measured" (dashed) relative angle distributions are shown in Fig. 12 for both the sequential evaporation and fission simulations. The raw distributions differ from those in Figs. 2 and 4 in that now they are associated with a distribution of projectile excitation energies. This washes out some of the structure which is evident in Figs. 2 and 4, but the large peaks at $\beta \approx 10°$ which correspond to pairs of alpha particles produced from the decay of the ground state of ^{8}Be are still evident. However in

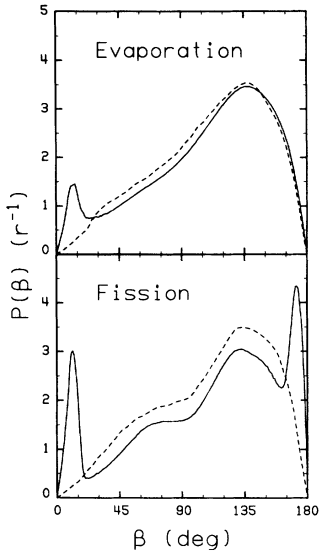

FIG. 12. Relative angle distributions predicted for the ^{16}O+^{159}Tb reaction with the sequential evaporation and the sequential fission simulations assuming an initial angular momentum of $I = 0\hbar$. The primary distributions are indicated by the solid curves and the reconstructed distributions of events which were completely "detected" in the simulated detector are indicated by the dashed curves.

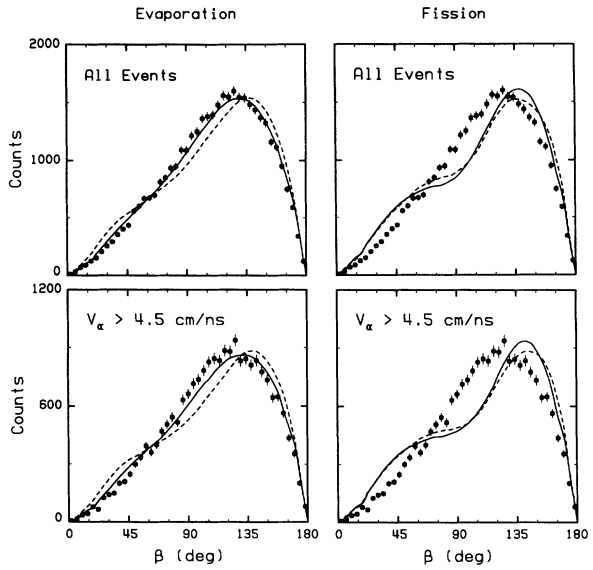

FIG. 13. Experimental relative angle distributions (data points) compared to predictions from the sequential evaporation and the sequential fission simulations (curves). The top two experimental distributions are identical and were obtained for all selected ^{16}O→4α events and the bottom two distributions for events where all four alpha particles have laboratory velocities greater than 4.5 cm/ns. The dashed and solid curves were obtained from the simulations assuming initial angular momenta of $I = 0\hbar$ and $5\hbar$, respectively.

the laboratory frame, the relative angle between such a pair is even smaller and both alpha particles generally enter the same detector and the event is rejected. These peaks are thus absent from the reconstructed distributions. Also the peak at the largest relative angles in the sequential fission simulation is removed as it is also associated with these rejected events. The conclusions of this work thus refer mostly to the decay channels where ^{8}Be intermediates are formed in excited states. Futhermore, prompt-like decay events, where alpha particles interact via resonant scattering through the ground state of ^{8}Be, will also be rejected.

The experimental relative angle distributions are compared to simulated "measured" distributions in Fig. 13 for $0\hbar$ and $5\hbar$ of initial ^{16}O angular momentum. The simulated distributions have been normalized to the same number of selected events as the experimental distribution. Relative distributions are shown for all selected events and for those events where all the alpha particle laboratory velocities are greater than 4.5 cm/ns. The second group of events are less likely to be contaminated by incorrectly identified events (Sec. IV B). However, the experimental relative angle distributions are almost identical for both groups of events. Because of the sensitivity of some of the simulations to the projectile excitation energy, the distributions of reconstructed projectile excitation energy are shown in Fig. 14. The thick-lined histogram was obtained from all of the selected events and the thin-lined histogram results when the extra velocity criterion was imposed. The mean reconstructed projectile excitation energy is approximately 40 MeV and the shape is similar to that obtained by Pouliot *et al.* (see Fig. 8 of Ref. [8]). The shape of the relative angle distributions obtained by these authors [2] is also in good agreement with those of this work.

None of the predicted distributions obtained from the fission simulations reproduced the experimental distributions in Fig. 13. In contrast, the predictions from the sequential evaporation simulation give a much better reproduction of the data. Specifically, the $I = 5\hbar$ prediction, indicated by the solid curve, fits the data very well. Owing to large CPU time requirements for these simulations with quantum mechanical treatment of correlations, no search was performed for the value of I which produces the best fit to the data. However, from the simulations using semiclassical treatment of correlations,

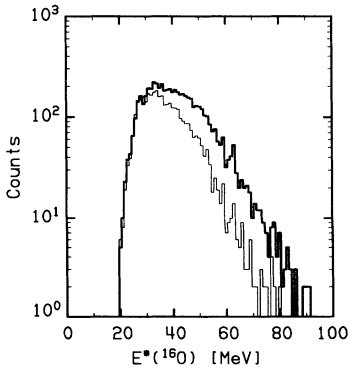

FIG. 14. Same as for Fig. 8, for the reconstructed projectile excitation energy.

the dependence of the predicted relative angle distribution on projectile angular momentum decreases rapidly as I is increased past $5\hbar$. From this, it is concluded that the value of I which is consistent with data is of the order of $5\hbar$ or larger.

The above conclusions refer, of course, to spectra of projectile excitation energies sampled in the experimental relative angle distributions. It may be possible for the fission decay mechanism to be a dominant mechanism at the highest projectile excitation energies. To investigate this possibility, the relative angle distributions for three gates on the reconstructed projectile excitation energy were obtained. As all the distributions have the same general shape, differences between the distributions can be highlighted by dividing each distribution by one such representative distribution. To this end, the experimental and simulated relative angle distributions were divided by the distribution obtained with the random simulations. Figure 15 compares the resultant experimental and simulated distributions for the three gates on reconstructed projectile excitation energy.

The sequential evaporation simulation with $I = 5\hbar$ gives the best fit of all the predicted distributions to the data at all three excitation energy gates. Although for the highest excitation energy gate (E^*>50 MeV), the sensitivity of the predictions to the initial angular momentum or to the decay mechanism is diminished. For this gate, the predictions from the sequential evaporation simulation differ only by the presence of a "kink" at $\beta \approx 30°$ for $I = 5\hbar$. However, this kink is consistent with the experimental data. A kink at slightly larger values of β is also predicted with $I = 5\hbar$ for the other excitation energy gates and these kinks are in good agreement with the experimental data. The sequential fission simulations fail to reproduce the experimental data for all three excitation energy gates, although for E^*>50 MeV, where the predictions are closest to the experimental data, it is difficult to exclude some small fraction of sequential fission events. However, over the range of projectile excitation energies sampled in this work, the relative angle distributions for the four alpha particle exit channel are well described by the sequential evaporation of these particles. Owing to the difficulty in calculating four-body correlations for simultaneously emitted alpha particles, no predictions are presented for prompt decay scenarios. The extent to which the experimental relative angle distributions are consistent with prompt decay modes, either dynamical or statistical, for which α-α interactions are important is still an open question.

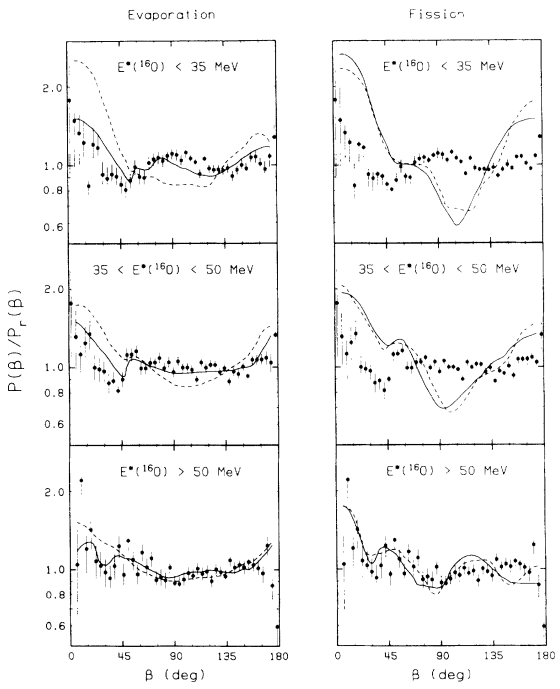

FIG. 15. Relative angle distributions $P(\beta)$ divided by the corresponding predictions obtained from the random simulation $P_r(\beta)$ for the three indicated bins of the reconstructed projectile excitation energy. The experimental results (data points) are compared to predictions of the sequential evaporation and the sequential fission simulations assuming initial angular momenta of $I = 0\hbar$ (dashed curves) and $I = 5\hbar$ (solid curves).

Note that the highest excitation energy bin (E^*>50 MeV) contains significant numbers of events where at least one alpha particle's laboratory velocity is less than 4.5 cm/ns. This can be seen from Fig. 14. There was some concern as to whether some of these events were correctly identified as $^{16}O \rightarrow 4\alpha$ events in Sec. IV B and could be 4α events containing some alpha particles emitted from the target nucleus. The relative angle distribution for such events may be similar to the random distribution as more of the alpha particles pairs are uncorrelated. This distribution would correspond to a constant value of unity in Fig. 15. A substantial contamination of such events should wash out the kink predicted by the sequential evaporation simulation ($I = 5\hbar$). As this kink is still present in the experimental distribution, then there is no evidence of any significant contamination. The low multiplicities of coincident light particles detected in the back of the Ball for these events (Sec. IV B) probably reflect the fact that the interaction between the target and projectile is not two body. In view of the fact that there may be a non-evaporative component of light charged particles emitted from the target (Sec. IV A), it would not be surprising to find a similar component for neutrons. The presence of such neutrons, probably emitted during the interaction of the target and the projectile, would reduce the excitation energy which was assigned to the target in the Monte Carlo simulations. The predicted multiplicities of particles evaporated from the target would thus be reduced giving a closer agreement with the experimental values.

C. Target proximity effect

A search for an anisotropy in the in-plane emission of the alpha particles was performed to determine if the decay of the projectile took place in the Coulomb field of the target nucleus. The momentum tensor of Eq. (6) was constructed for the same three bins of projectile excitation energy as used in the previous section. Before any

information on the target proximity effect can be determined, the anisotropy induced by the incomplete angular coverage of the detector array and the event selection criteria must be removed. The momentum tensor was determined in simulations without any proximity effect, for all events ($\mathbf{T}_{\rm all}$) and for reconstructed events which passed the event selection criteria ($\mathbf{T}_{\rm filtered}$). The inclusion of the instrumental biases in the simulation induced a strong in-plane distortion for the reconstructed events. This is illustrated in the upper panel of Fig. 16 for the three bins of projectile excitation energy. Here the in-plane projections of the ellipsoids of the momentum tensors $\mathbf{T}_{\rm filtered}$ are shown. The projection is an ellipse with the semimajor and semiminor axes orientated according to the directions of the two in-plane eigenvectors with their lengths corresponding to the respective eigenvalues. Projections are shown in Fig. 16 (upper panel) for three values of aligned angular momentum (solid curves). The orientation of the distortion remains unaffected by the magnitude of the angular momentum. The area of the ellipse increases with increasing I as in-plane emission becomes more favored. Also the eccentricity of the ellipse shows a small dependence on I. In comparison to these simulated results, the projections obtained from the experimental events are indicated by the dashed-lined ellipses. Two of its eigenvectors were also found to lie in the reaction plane. Its distortion is orientated at a different angle to those from the simulation and could not be reproduced by varying the amount of aligned angular momentum.

The instrumental distortion was removed by a correction transformation $\mathbf{C}$ giving the corrected momentum tensor:

$$\mathbf{T}_{\rm corr} = \mathbf{C}^T \mathbf{T}_{\rm raw} \mathbf{C} \tag{8}$$

where $\mathbf{T}_{\rm raw}$ is the momentum tensor obtained directly from the reconstructed experimental data. The transformation $\mathbf{C}$ was defined such that for the simulations, $\mathbf{T}_{\rm all} = \mathbf{C}^T \mathbf{T}_{\rm filtered} \mathbf{C}$, where the amount of aligned angular momentum in the simulation was adjusted such that the out-of-plane eigenvalues of $\mathbf{T}_{\rm filtered}$ and $\mathbf{T}_{\rm raw}$ were equal. The projections for the corrected tensors are shown in the lower panel of Fig. 16. The ratios of the in-plane and out-of-plane eigenvalues and orientation of the residual distortion after correction are listed in Table I. The errors listed in Table I are standard errors associated with statistical fluctuations due to the finite number of events analyzed. They were estimated by performing 20 simulations each with the same number of events as for the experimental results and then analyzing these events in the same manner as for the experimental data to correct for the instrumental distortions. The errors quoted are the standard deviations of the results obtained from each of the 20 simulations. Apart from these statistical errors, the largest uncertainty in the results is associated with the correction of the instrumental distortion. The distortion induced by detector geometry and selection criteria is larger than that expected from the target proximity effect. Therefore, careful simulations of this detector bias are required. The degree to which this bias is determined should reflect the extent to which the simulations model the angle and velocity distributions of the projectile. As described in Sec. V A, considerable efforts were made in this regard. It is believed that the results listed in Table I are not due to some residual instrumental bias which was not fully removed. To some extent this belief is supported by the observation that the orientation of the instrumental distortion rotates towards negative angles with increasing excitation energy (see Fig. 16 upper panel) whereas the corrected momentum tensors show an in-plane distortion which rotates towards positive angles (see Fig. 16 lower panel).

The experimental momentum tensors are qualitatively consistent with some aligned angular momentum and with a perturbation due to the proximity of a target

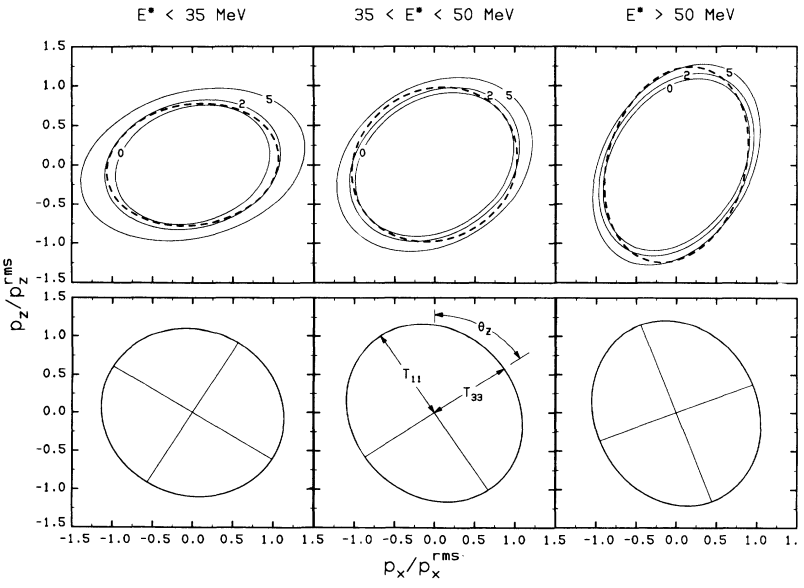

FIG. 16. Projections of the momentum tensor ellipsoid on the reaction plane for the three bins of reconstructed projectile excitation energy. In the upper panel, the solid-lined ellipses represent predicted momentum tensors obtained from the simulations taking into account the detector geometry and the event selection criteria. Predictions are shown for $I = 0\hbar$, $2\hbar$, and $5\hbar$ of aligned projectile angular momentum. The dashed-lined ellipses, in the upper panel, indicate the corresponding momentum tensors obtained from the experimental data. The projections in the lower panel are associated with the experimental momentum tensors after they were corrected for the instrumental distortion. Also the definitions of the angle θ_z and the eigenvalues T_{11} and T_{33} are illustrated.

TABLE I. Parameters of the experimental momentum tensors [Eq. (6)] obtained for three bins of reconstructed projectile excitation energy. The quantity R_{in} gives the ratio of the two in-plane eigenvalues of the tensors while the quantity R_{out} is the ratio of the out-of-plane and one of the in-plane eigenvalues (see text). The angle θ_z indicates the orientation of the in-plane eigenvectors relative to the z axis whereas the angle θ_y is between the out-of-plane eigenvector and the y axis.

$E^*(^{16}O)$ (MeV)	R_{in}	θ_z (deg)	R_{out}	θ_y (deg)
<35	0.92±0.07	32±21	0.69±0.02	3.7±2.2
35→50	0.86±0.03	56±3	0.66±0.02	0.6±1.5
>50	0.83±0.04	69±3	0.63±0.04	3.7±2.0

nucleus. These conclusions are the result of three observations: Firstly, for all excitation energy bins, two of the three eigenvectors are located in the reaction plane to within a few degrees and consequentially the other eigenvector is close to the y axis which is directly out of the reaction plane. In Table I, the angle between this eigenvector and the y axis is listed as θ_y. Secondly, the ratio R_{out} is less than unity for all bins indicating a preference for in-plane emission. This would be expected if the angular momentum of the projectile was, on average, aligned along the y axis. Lastly, the ratio R_{in} decreases and the angle θ_z increases as the projectile excitation energy increases. These trends are consistent with stronger Coulomb interactions between the target and the alpha particles with increasing excitation energy. Such trends are expected because with increasing excitation energy the projectile will decay closer to the target as its lifetime decreases and also the projectile-target separation velocity, on average, decreases.

To understand quantitatively the magnitude of the proximity effect, the data are compared to simulations which include the decay of the projectile in the Coulomb field of the target nuclei. These simulations are the same as discussed in Sec. II B only now the separation velocities between the target and projectile, after their interaction, are determined assuming the interaction is two body as in Sec. V A. The simulated events are passed through the detector filter and the resulting instrumental distortion is removed by correcting the momentum tensor [Eq. (8)] as is done for the experimental data. The values of R_{in} and θ_z obtained from these simulations are plotted as a function of the input parameter Γ, the decay width of the projectile, in Fig. 17 for the three excitation energy bins. The error bars shown on the predictions are statistical. Simulations were performed for $I = 0\hbar$ and $5\hbar$ and, in the latter case, for when the angular momentum is aligned out of the reaction plane and for random alignment. As in Sec. II B, the predicted values of R_{in} show little dependence on I or the amount of alignment whereas θ_z is larger when the angular momentum is aligned. The general trends of these predictions are indicated by the dashed curves. Note that when the value of R_{in} equals unity, the angle θ_z becomes undefined. Hence, as R_{in} approaches unity, the error associated with θ_z greatly increases.

The experimental data for each excitation energy bin in Fig. 17 are represented by three horizontal lines indicating the mean and the mean plus and minus one standard error. For the lowest excitation energy bin (E^*<35 MeV), the large error associated with the experimental value of R_{in} does not restrict the range of Γ. The experimental result is even consistent with no target proximity effect. For the higher excitation energy bins, the statistical error is small and a comparison with the simulated values of R_{in} suggests that the decay widths for these events are of the order from 5 to 10 MeV. For the intermediate excitation energy bin, the experimental value of θ_z is consistent with the simulated values obtained with an aligned $5\hbar$ of projectile angular momentum for the same range of Γ. The experimental value of θ_z for the highest excitation energy bin is larger than all the simulated values. However, it is expected that such a value could be obtained in the simulation by increasing the amount of aligned projectile angular momentum.

Before discussing the significance of the above results,

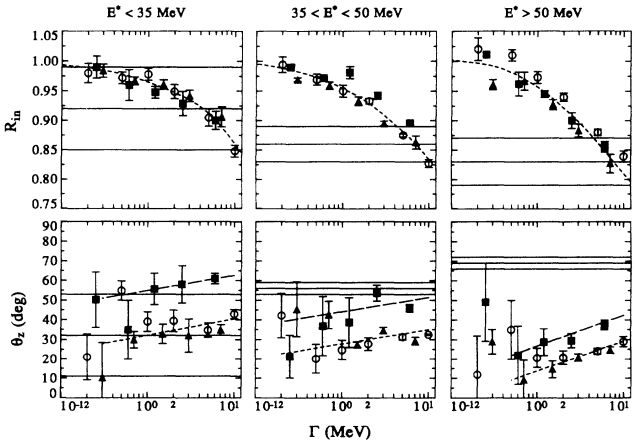

FIG. 17. The predicted dependence of the momentum tensor on the decay width of the projectile for three bins of projectile excitation energy. The quantity R_{in} is the ratio of the two in-plane eigenvalues of the momentum tensor while the angle θ_z is the orientation of these eigenvectors with respect to the z axis (see text). The predictions indicated by open circles are for zero angular momentum of the projectile, whereas the square and triangular points are associated with $5\hbar$ of angular momentum aligned, respectively, out of the reaction plane and isotropically. The error on the predictions are from the statistics of the simulations. The dashed curves, which are fits to the predictions, guide the eye. The experimental results are given by the horizontal lines which indicate the mean and the mean ±1 standard error.

it is worth noting the limitations of the simulations. (1) The simulations assumed a two-body interaction between the target and projectile to determine their initial separation velocity. As discussed in Secs. IV and V C, there are indications that this is not strictly true. If the separation velocity is smaller, then the projectile will stay in the target field longer and hence result in a larger effect. (2) The ^{159}Tb target nucleus is assumed to be spherical in the simulations and no account is taken of its deformation. If the simulations were averaged over target orientation, then it is expected that the predicted magnitude of the effect would increase. This effect has not been investigated quantitatively. (3) The initial emission direction of the alpha particles was assumed unaffected by the target field. However, it is possible that the target field affects the decay process itself resulting in an initial anisotropic emission pattern even before the alpha particles have moved away from the projectile. Here again, the simulations would have underestimated the magnitude of the effect.

In view of these considerations, the decay widths may be less than the range of 5 to 10 MeV obtained from the comparison with the simulations. In any case, the observation of any target proximity effect at all indicates that the projectile starts decaying very quickly after the interaction with the target nucleus. A decay width of 5 MeV corresponds to a time interval of approximately 10^{-22} s. Also if the decay width for the emission of the second alpha particle is of similar order, then it will be important to consider final state interactions between the alpha particles. This raises some questions as to the validity of the conclusion drawn from the relative angle distributions in Sec. II A as no interactions between the alpha particles were considered in those simulations. Figure 18 shows simulated relative angle distributions obtained with the inclusion of the target proximity effect for Γ=5 MeV and $I = 5\hbar$ (solid curve). There is only a small dependence of the relative angle distributions on the alignment of the projectile angular momentum. These simulations include Coulomb interactions of the target with the alpha particles and also Coulomb interactions between the alpha particles. As in Sec. II B, the decay width for the ^{12}C intermediate was taken to be the same as for the ^{16}O fragment. For comparison, the distribution obtained without these interactions (dashed curve) and the experimental data are also shown. The main difference between the predictions, with and without interactions, can be attributed to the interactions between the alpha particles themselves. The interactions between the alpha particles and the target have a much smaller effect on the relative angle distributions. However, the effect of including the interactions between the alpha particles is similar to that obtained by increasing the projectile angular momentum in Fig. 15, i.e., it decreases the number of small and large relative angles while increasing the number of intermediate angles. As such, it would be difficult to determine both the projectile angular momentum and its decay width from relative angle distributions alone. Although the fit to data in Fig. 18 is worse when interactions are included, one should note that the simulations were performed using the semiclassical treatment of correlations. A corresponding simulation with the quantum mechanical treatment of the correlations, but no target proximity effect, is indicated by the solid curve ($I = 5\hbar$) in the middle-left panel of Fig. 15. The quantum mechanical treatment of correlations results in more relative angles near β=0° and 180° than the equivalent semiclassical treatment. Also in this regard, it should be noted that when the time interval between alpha particle emissions is small, proper treatment of the final state interactions between these particles should include resonance scattering and other effects associated with the α-α interaction in addition to their Coulomb repulsion (Sec. II A).

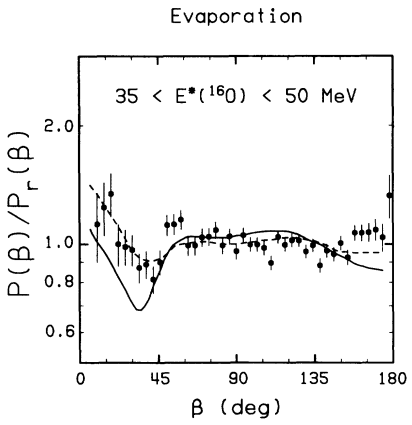

FIG. 18. Normalized relative angle distributions for the reconstructed projectile excitation energy bin (35 $<E^*<$50 MeV). The solid circles indicate the experimental results while the curves were obtained from sequential evaporation simulations with $I = 5\hbar$. The solid curve indicates the predictions when Coulomb interactions between the alpha particles and between an alpha particle and the target nucleus are included (see text). In comparison, the dashed curve was obtained from a simulation which did not include interactions.

D. Pickup and direct reactions

In the above analyses it is also important to consider neutron pickup reactions leading to the formation of excited ^{17}O fragments. If such fragments disassemble into four alpha particles and a neutron then it will be impossible to differentiate them from ^{16}O$\rightarrow 4\alpha$ events in this study as neutrons were not detected. Neutron pickup reactions were found to be quite important for ^{16}O + ^{179}Au reactions at similar bombarding energies to that used in this study [26, 27] and thus these events may contaminate the selected event sample used in the relative angle analysis. In the statistical model, an excited ^{17}O fragment is expected to decay predominantly by neutron emission leading to an ^{16}O intermediate or residue. If the 4α events studied in this work arise from the decay of the ^{16}O intermediate, then the reconstructed quantities such as the excitation energy and velocity and conclusions about the decay width and angular momentum are associated with the intermediate and not the primary

^{17}O fragment. Otherwise, the conclusions of this work are still valid. Of course there will be some probability for the neutron to be emitted later in the decay sequence. If the decay sequence includes a ^{9}Be rather than a ^{8}Be intermediate, then the predicted relative angle distribution will be affected. Firstly, the peaks associated with ^{8}Be decay will be missing, and secondly, the correlations between emission directions will be lost. The relative angle distribution will be more similar to that obtained in the simulation of Sec. II A with no correlations between emission directions and with Fermi gas level densities for the ^{8}Be intermediate. This was shown to be almost identical with the results of the random simulation. However, as the random simulation does not reproduce the experimental relative angle distributions as well as the sequential evaporation simulation, most 4α events are probably associated with a ^{8}Be intermediate.

Charged particle pickup reactions may also be important in this study, but are less likely to contaminate the event sample as the selection criteria rejects events where four alpha particles and an additional charged particle are detected in the Wall counters. However, some charged particle pickup reactions may be incorrectly identified if the additional charged particle is not detected. To investigate the possible magnitude of this incorrect identification, analyses were performed for events where five alpha particles or four alpha particles plus a proton were detected in the Wall counters. The number of these events was only 4% and 15%, respectively, of the number of selected $^{16}\mathrm{O}\rightarrow 4\alpha$ events. Now the probability of detecting the extra particle in the Wall counters is expected to be greater than 50% and thus the percentages of incorrectly identified events will be less than the above values. Also not all of these events, with an additional charged particle, will be associated with pickup reactions as the extra particle may well have been evaporated from the target nucleus. Therefore, these percentages must be considered as maximum values for contamination by charged particle pickup reactions.

The time scale extracted for the emission of the first alpha particle is approaching the time scale for direct reactions. This may suggest a disassembly scenario where the projectile breaks up promptly into an alpha particle and an excited ^{12}C fragment during its interaction with the target after which the ^{12}C fragment decays by statistical alpha particle emission. However, it should be noted that in extracting the decay width of the projectile, it was assumed that the first alpha particle is emitted statistically, i.e., the initial in-plane momentum distribution is isotropic and only became anisotropic due to Coulomb interactions with target nucleus. If the first alpha particle is emitted promptly, then the initial in-plane distribution may not be isotropic. A similar situation applies for dynamical models such as Ref. [28] where all the alpha particles may be produced in a direct reaction. Further theoretical work should address the question whether direct breakup models can reproduce the observed magnitude and orientation of the momentum anisotropy.

VI. SUMMARY

The decay of excited projectiles produced in the reaction $E/A = 25$ MeV ^{16}O + ^{159}Tb into four alpha particles has been studied. The alpha particles and light charged particles evaporated from the target nucleus were detected with a large array of counters covering nearly 4π in solid angle. Candidate events associated with the $^{16}\mathrm{O}\rightarrow 4\alpha$ decay were chosen by selecting events with four, and only four, alpha particles detected in the forward (Wall) array ($4^\circ \lesssim \theta_{\mathrm{lab}} \lesssim 32^\circ$). The multiplicities and angular distributions of coincident light charged particles detected in the backward (Ball) array were investigated and compared to expectations for statistical emission from the target nucleus.

The distribution of relative angles between the four alpha particles were presented and compared to simulations assuming either the sequential evaporation of alpha particles from the projectile or the fission of the projectile into two ^{8}Be fragments which subsequently decay. The simulations took into account the known levels of ^{8}Be and correlations between emission directions of the various particles. The experimental distributions were found to be inconsistent with the fission simulations. However for projectile angular momenta of the order of $5\hbar$ or larger, the sequential evaporation simulation reproduced the data over the whole range of excitation energies sampled in the experiment ($E^*/A \lesssim 4.5$ MeV).

The momentum distribution of the alpha particles was examined. The distribution showed a preference for alpha emission in the reaction plane consistent with some aligned projectile angular momentum. For the higher projectile excitation energies, the in-plane momentum distribution was found to be anisotropic about the projectile center of mass. Monte Carlo simulations including Coulomb interactions between the first emitted alpha particle and the target nucleus were able to reproduce this effect if the lifetime of the projectile was of the order of 10^{-22} s.

In conclusion, the 4α exit channel is consistent with the disassembly of the projectile by the sequential emission of α particles. For the higher excitation energies, the first α particle is emitted very soon after the end of the target-projectile interaction. Further theoretical work is needed to determine whether the data are consistent or inconsistent with prompt decay mechanisms, either statistical or dynamical.

ACKNOWLEDGMENTS

J.B. wishes to acknowledge travel expenses provided by CNPq, Brazil. This work was supported by the Office of Energy Research, Office of High Energy and Nuclear Physics, Nuclear Physics Division of the U.S. Department of Energy, under Contract Nos. DE-FG02-87-ER40316 and DE-FG02-88-ER40406. Oak Ridge National Laboratory is managed by Martin Marietta Energy Systems, Inc. under Contract No. DE-AC05-84OR21400 with the Department of Energy.

[1] R. Trockel *et al.*, Phys. Rev. Lett. **59**, 2844 (1987).
[2] B.A. Harmon *et al.*, Phys. Lett. B **235**, 234 (1990).
[3] J. Suro *et al.*, Lawrence Berkeley Laboratory Report LBL-31957.
[4] D.A. Cebra *et al.*, Phys. Rev. Lett. **64**, 2246 (1990).
[5] J.A. López and J. Randrup, Nucl. Phys. **A491**, 477 (1989).
[6] P. Danielewicz and M. Gyulassy, Phys. Lett. **129B**, 283 (1983).
[7] P. Glässel, D.v. Harrah, H.J. Specht, and L. Grodzins, Z. Phys. A **310**, 189 (1983).
[8] J. Pouliot *et al.*, Phys. Rev. C **43**, 735 (1991).
[9] F. Ajzenberg-Selove, Nucl. Phys. **A506**, 1 (1990).
[10] F. Ajzenberg-Selove, Nucl. Phys. **A490**, 1 (1988).
[11] L.C. Biedenharn, G.B. Arfken, and M.E. Rose, Phys. Rev. **83**, 586 (1951).
[12] L.C. Biedenharn and M.E. Rose, Rev. Mod. Phys. **25**, 729 (1953).
[13] S.E. Koonin, Phys. Lett. **70B**, 43 (1977).
[14] S. Pratt and M.B. Tsang, Phys. Rev. C **36**, 2390 (1987).
[15] W.G. Gong, W. Bauer, C.K. Gelbke, and S. Pratt, Phys. Rev. C **43**, 781 (1991).
[16] B. Buck, H. Friedrich, and C. Wheatley, Nucl. Phys. **A275**, 246 (1977).
[17] S. Ali and A.R. Bodmer, Nucl. Phys. **80**, 99 (1966).
[18] D.W. Stracener *et al.*, Nucl. Instrum. Methods **A294**, 485 (1990).
[19] An analysis of the events was performed where the assigned angle was chosen randomly over the face of the detector as in Refs. [2, 8]; however, the final results were similar and the conclusions identical.
[20] J.M. Alexander, M.T. Magda, and S. Landowne, Phys. Rev. C **42**, 1092 (1990).
[21] D. Wilmore and P.E. Hodgson, Nucl. Phys. **55**, 673 (1964).
[22] F.G. Perey, Phys. Rev. **131**, 745 (1963).
[23] J.R. Huizenga and G. Igo, Nucl. Phys. **29**, 462 (1962).
[24] J.M. Lohr and W. Haeberli, Nucl. Phys. **A232**, 381 (1974).
[25] C.M. Perey and F.G. Perey, At. Data Nucl. Data Tables **17**, 1 (1976).
[26] M. Bini *et al.*, Phys. Rev. C **22**, 1945 (1980).
[27] S.B. Gazes *et al.*, Phys. Lett. B **208**, 194 (1988).
[28] K. Möhring, T. Srokowski, and D.H.E. Gross, Nucl. Phys. **A533**, 333 (1991).